Biochemical and Biophysical Research Communications 432 (2013) 141–145

Contents lists available at SciVerse ScienceDirect

Biochemical and Biophysical Research Communications

journal homepage: www.elsevier.com/locate/ybbrc

Spatial arrangement and functional role of α subunits of proteasome activator PA28 in hetero-oligomeric form

Masaaki Sugiyama [a,*], Hiroki Sahashi [b], Eiji Kurimoto [b,c], Shin-ichi Takata [d], Hirokazu Yagi [b], Keita Kanai [b], Eri Sakata [b], Yasufumi Minami [e], Keiji Tanaka [f], Koichi Kato [b,g,h,*]

[a] Research Reactor Institute, Kyoto University, Osaka 590-0494, Japan
[b] Graduate School of Pharmaceutical Sciences, Nagoya City University, Nagoya 467-8603, Japan
[c] Faculty of Pharmacy, Meijo University, Nagoya 468-8503, Japan
[d] J-PARC Center, Japan Atomic Energy Agency, Ibaraki 319-1195, Japan
[e] Department of Biotechnology, Maebashi Institute of Technology, Gunma 371-0816, Japan
[f] Tokyo Metropolitan Institute of Medical Science, Tokyo 156-8506, Japan
[g] Okazaki Institute for Integrative Bioscience, National Institutes of Natural Sciences, Okazaki, Aichi 444-8787, Japan
[h] Institute for Molecular Science, National Institutes of Natural Sciences, Okazaki, Aichi 444-8787, Japan

ARTICLE INFO

Article history:
Received 16 January 2013
Available online 29 January 2013

Keywords:
PA28
Proteasome
Small-angle neutron scattering
Deuteration
Major histocompatibility complex class I molecule
Degradation

ABSTRACT

A major form of proteasome activator PA28 is a heteroheptamer composed of interferon-γ-inducible α and β subunits, which share approximately 50% amino acid identity and possess distinct insert loops. This activator forms a complex with the 20S proteasome and thereby stimulates proteasomal degradation of peptides in an ATP-independent manner, giving rise to smaller antigenic peptides presented by major histocompatibility complex class I molecules. In this study, we performed biophysical and biochemical characterization of the structure and function of the PA28 hetero-oligomer. Deuteration-assisted small-angle neutron scattering demonstrated three α and four β subunits are alternately arranged in the heptameric ring. In this arrangement, PA28 loops surround the central pore of the heptameric ring (site for peptide entry). Activating the 20S proteasome with a PA28 mutant that lacked the α subunit loops cleaved model substrates longer than a nonapeptide with better efficiency when compared to wild-type PA28. Based on these data, we hypothesize that the flexible PA28 loops act as gatekeepers, which function to select the length of peptide substrates to be transported between the proteolytic chamber and the extra-proteasomal medium.

1. Introduction

The 20S proteasome is part of the protein degradation machinery of the cell and has a cylindrical structure, which sequesters two proteolytic chambers located in a symmetrically related manner [1,2]. Proteolytic functions of this molecular machine are promoted through its interaction with other protein complexes, which are termed proteasome activators (PAs) [3]. PA700, which is composed of at least 19 different subunits, mediates proteasomal degradation of ubiquitinated proteins in an ATP-dependent manner. Another protein complex, PA28 (also known as REG and the 11S regulator) activates ATP-independent proteasomal proteolysis of small peptides [4,5]. These PA complexes harbor several subunits that contain C-terminal proteasome-binding motifs, which allow docking onto the ends of the proteasome cylinder. As a result of PA binding, the proteasome gate that normally restricts the unregulated access of substrates, are now permeable for the substrates to enter the active sites in the proteolytic chamber [3].

While three homologs (α, β, and γ) have been identified as subunits of PA28, the major form of this proteasome-activating complex is a heteroheptamer composed of the α and β subunits (hereafter, termed PA28α and PA28β, respectively). Expression of these subunits is induced by interferon-γ (IFN-γ) in a variety of cells and associated with efficient production of antigenic peptides presented by major histocompatibility complex (MHC) class I molecules [6–10]. Although PA28α and PA28β share approximately 50% amino acid identity, they each possess a distinct insert region

Abbreviations: DTT, dithiothreitol; HSQC, heteronuclear single-quantum coherence; IFN-γ, interferon-γ; MHC, major histocompatibility complex; PA, proteasome activator; SANS, small-angle neutron scattering; TRP2, tyrosinase-related protein-2.

* Corresponding authors. Addresses: Division of Quantum Beam Material Science, Research Reactor Institute, Kyoto University, 2-1010 Asashiro-nishi, Kumatori, Sennan, Osaka 590-0494, Japan. Fax: +81 72 451 2670 (M. Sugiyama). Okazaki Institute for Integrative Bioscience, National Institutes of Natural Sciences, 5-1 Higashiyama, Myodaiji, Okazaki 444-8787, Japan. Fax: +81 564 59 5224 (K. Kato).

E-mail addresses: sugiyama@rri.kyoto-u.ac.jp (M. Sugiyama), kkatonmr@ims.ac.jp, kkato@phar.nagoya-cu.ac.jp (K. Kato).

0006-291X/$ - see front matter © 2013 Elsevier Inc. All rights reserved.
http://dx.doi.org/10.1016/j.bbrc.2013.01.071

that differs in length and sequence (Supplementary Fig. S1). Reportedly, the PA28α insert is dispensable for proteasome binding and activation and removal of the PA28β insert results in reduced proteasome activation [11,12]. Thus, PA28α and PA28β contribute to the regulation of proteasomal functions in different ways.

A crystallized, conical structure has been reported for a homoheptameric ring of the human PA28α, but lacked interpretable electron density corresponding to the inserts due to structural disorder of these segments [13]. In our previous study, we used small-angle neutron scattering (SANS) to characterize the solution structure of mouse PA28 formed from wild-type PA28β and a mutated PA28α that lacked the insert [14]. The SANS data indicated that these subunits formed heteroheptameric rings, parts of which were stacked back to back to form a double-ring structure, but could not provide any information on spatial arrangements of the subunits due to their structural similarity.

In the present study, we attempted to address this issue by PA28α-selective deuteration of wild-type PA28 in conjunction with contrast-matching SANS measurements. Post inspecting the deuteration-assisted SANS data, we propose a 3D model of the PA28 oligomeric structure. We also discuss the functional role of the PA28α insert based on biochemical data obtained through analysis of a series of model peptides.

2. Materials and methods

2.1. Preparation of PA28

The cDNAs of mouse PA28α and PA28β were sub-cloned into the expression vectors pET21d and pET23a, respectively. A PA28α mutant in which the insert segment (Val69 to Lys97) substituted with a glycine-serine dipeptide was constructed as previously described [14]. The wild-type and mutated PA28α and PA28β were separately expressed in *Escherichia coli* strain BL21-CodonPlus (Stratagene) and purified as described [14]. For the preparation of perdeuterated PA28α, bacteria were grown in M9 minimal media containing deuterated glucose (2 g/L) and 99.8% D_2O. Uniformly ^{15}N-labeled PA28α was expressed by cultivating bacterial cells in M9 minimal medium that contained [^{15}N]NH_4Cl. The hetero-oligomer of PA28 was constructed by mixing either wild-type or mutated PA28α (final protein concentration of 0.1 mg/mL) with approximately one molar equivalent of wild-type PA28β followed by dialysis against 20 mM Tris-HCl buffer (pH 7.6) containing 20 mM NaCl, 1 mM EDTA, 5 mM 2-mercaptoethanol, and 5% glycerol (4 °C for 24 h). Hetero-oligomers were then purified by gel filtration chromatography using a Superose 12 column (GE Healthcare Life Sciences). Hereafter, the wild-type PA28 oligomer and the PA28 oligomer composed of the PA28α mutant and wild-type PA28β will be designated as $PA28_{wt}$ and $PA28_{\Delta\alpha loop}$, respectively. Complex formation between the 20S proteasome–recombinant PA28 protein was checked by native polyacrylamide gel electrophoresis.

2.2. SANS measurement

The SANS experiments were performed using a SANS2d spectrometer, a newly launched time-of-flight SANS spectrometer dedicated to the long pulse neutron source at target station 2 of ISIS (neutron scattering facility) at Rutherford Appleton Laboratory, Didocot, UK [15]. The total q-range covered with the spectrometer was 0.002-2 $Å^{-1}$. The quaternary structure of $PA28_{wt}$ was analyzed by the contrast variation method [16–18]. $PA28_{wt}$ composed of perdeuterated PA28α and non-deuterated (natural abundance) PA28β was subjected to SANS measurement in 50 mM Tris-HCl (pH 7.5) containing 1 mM dithiothreitol (DTT) and a variable amount of D_2O at a protein concentration of 5 mg/mL. The measurement time was 4 h and temperature was kept constant at 25 °C. The observed intensity was converted to a scattering profile in absolute unit via standard procedure.

2.2.1. 3D structure modeling

For simulation of the SANS profile of $PA28_{wt}$, its 3D-structural models were developed on the basis of homology modeling using the crystal structure of the PA28α homoheptameric ring (PDB code: 1avo) as described previously [13,14]. Depending on the configuration of PA28α and PA28β in each model, one or more PA28α subunit(s) in the crystal structure was/were replaced by the homology-modeled PA28β subunit(s), and the remaining PA28α subunit(s) was/were considered as deuterated. The loop inserts were represented by a sphere at the small basal plane, with scattering length equal to the sum of those ascribed to the loops in our modeling simulation.

2.3. In vitro proteasome proteolysis assay

As model proteasomal substrate, we used 9–24-mer peptides derived from RLAkt12–35 (denoting the peptide of altered Akt amino acid sequence ^{12}AYREETLSIIPGLPLSLGATDTMN^{35} in BALB/c RL♂1 cells), which contains the immunodominant H-2L^d-restricted precursor epitope, pRL1b [19]. A plasmid vector that contained the RLAkt peptide gene produced primer–dimer amplification was constructed and cloned as a fusion protein with hexahistidine-tagged ubiquitin (His_6–Ub) using a pET28a(+) vector (Novagene), which was transformed into *E. coli* strain BL21-CodonPlus. The bacterial cells were grown at 37 °C in Luria–Bertani medium containing 15 μg/mL of kanamycin. Protein expression was induced by adding 0.5 mM isopropyl-β-D-thiogalactopyranoside when absorbance reached 0.9 at 600 nm. After 5 h, cells were harvested, suspended in 50 mM Tris-HCl (pH 8.0), and subsequently disrupted by sonication. After centrifugation, the His_6-tagged protein was purified using a Chelating Sepharose Fast Flow column (GE Healthcare Life Sciences). The RLAkt peptide was enzymatically cleaved from the His_6–Ub moiety using recombinant glutathione S-transferase-tagged yeast ubiquitin hydrolase-1 as described previously [20] and subsequently purified by reverse-phase chromatography using a C8 column (Sunniest C8, CronTech) with a linear acetonitrile gradient.

Proteolysis of RLAkt peptides by the PA28-activated 20S proteasome was monitored according to the literature [21]. After addition of 0.1% TFA at the indicated time points, reaction mixtures were subjected to HPLC analysis using a C8 column and absorbance at 214 nm was monitored with a linear acetonitrile gradient. Amino acid sequence was determined by matrix-assisted laser desorption/ionization time-of-flight (TOF) mass spectrometric analyses using an AXIMA–CFR mass spectrometer (Shimadzu). A 21-mer peptide corresponding to residues 355–375 of mouse melanoma tyrosinase-related protein-2 ($TRP2_{355-375}$) was also used as model substrate [22]. The $TRP2_{355-375}$ peptide was prepared as His_6–Ub fusion and isolated according to the protocol used for the preparation of the RLAkt peptides. Degradation of a fluorogenic peptide N-succinyl-LLVY-amido-4-methycoumarin (Sigma) was monitored by time-course measurements of fluorescence intensity at 460 nm with excitation at 380 nm using spectrofluorophotometer (F-4500, Hitachi).

2.4. NMR measurement

$PA28_{wt}$ and $PA28_{\Delta\alpha loop}$ were dissolved in 50 mM potassium phosphate (pH 6.9) containing 10% D_2O at a protomer concentration

of 0.1 mM. $^{1}H–^{15}N$ HSQC spectra were measured at 30 °C using a Bruker DMX-500 spectrometer equipped with a cryogenic probe.

3. Results and discussion

3.1. Subunit composition of PA28

Prior to determination of the spatial arrangements of PA28α and PA28β in $PA28_{wt}$, we estimated their stoichiometric numbers in the complex. For this purpose, we focused on the neutron scattering length density (ρ_p) of $PA28_{wt}$ formed of deuterated PA28α. We calculated ρ_p for each of the eight possible models of $PA28_{wt}$, corresponding to incorporation of different numbers of deuterated PA28α subunits (i.e., 0–7 PA28α subunits in one heptameric ring). As shown in Supplementary Fig. S2A, the ρ_p value (and the corresponding D_2O ratio) increased depending on the number of deuterated PA28α since deuterium and hydrogen have positive and negative scattering lengths, respectively. Hence, the matching point, at which the scattering constant (defined as the difference in scattering length density of solvent and ρ_p) is expected to be null, also depends upon the number of deuterated PA28α contained in the heptameric ring.

To experimentally determine the matching point, we measured the zero angle scattering intensity $I(0)$, which is proportional to the square of the scattering contrast, for the $PA28_{wt}$ complex composed of perdeuterated PA28α and non-deuterated PA28β at varying H_2O/D_2O ratios. The matching point of this complex was 73.2 ± 2.8% D_2O (Supplementary Fig. S2B), indicating that the $PA28_{wt}$ heptamer was composed of three PA28α and four PA28β subunits. This is consistent with the electrospray ionization TOF mass spectrometric data of recombinant human PA28 [23].

3.2. Subunit arrangement of PA28

In determining the subunit arrangement of $PA28_{wt}$, we assumed two extreme models of its heptameric ring configuration (Supplementary Fig. S3): In one model, three PA28α and four PA28β subunits were segregated forming isologous clusters in the single ring as in the αααββββ configuration (designated as SR^c), while in the other model, the PA28α and PA28β subunits were alternately arranged with the exception of an adjacent PA28β–PA28β pair (i.e., βαβαβαβ, designated as SR^a). To generate double ring models, two single rings with identical subunit arrangement were combined so as to be related by a two-fold axis and associated in a back-to-back manner (Supplementary Fig. S3). In combining two SR^c rings, a two-fold axis was selected to render PA28α clusters that were most proximal and most distal between the rings thereby, giving DR^{cp} and DR^{cd} models, respectively. On the other hand, two SR^a rings were combined to render the PA28β–PA28β pair in the heptameric ring most distal between the two rings, giving DR^a model.

Based on these models, SANS profiles were simulated at three contrasting points (i.e., 0%, 40% and 98% D_2O). The simulations indicated that, although the DR^{cp} and DR^{cd} models gave quite similar SANS profiles, the DR^a model exhibited qualitatively distinct SANS profiles at 40% and 98% D_2O, which is characterized by a peak at $q \sim 0.13$ Å^{-1} (Supplementary Fig. S4). Because scattering contrasts of non-deuterated PA28β in 40% D_2O and deuterated PA28α in 98% D_2O are expected to be very low, SANS profiles measured under these conditions sensitively reflect the subunit arrangement of PA28. The experimentally observed SANS profiles exhibited a peak at $q = 0.13$ Å^{-1} in all scattering contrasts (Fig. 1), indicating that the DR^a model provided the best approximation of the hetero-oligomeric structure of $PA28_{wt}$. This is consistent with previously reported chemical cross-linking data, which identified the presence of PA28α–PA28β and PA28β–PA28β dimers but not of PA28α–PA28α dimers [23].

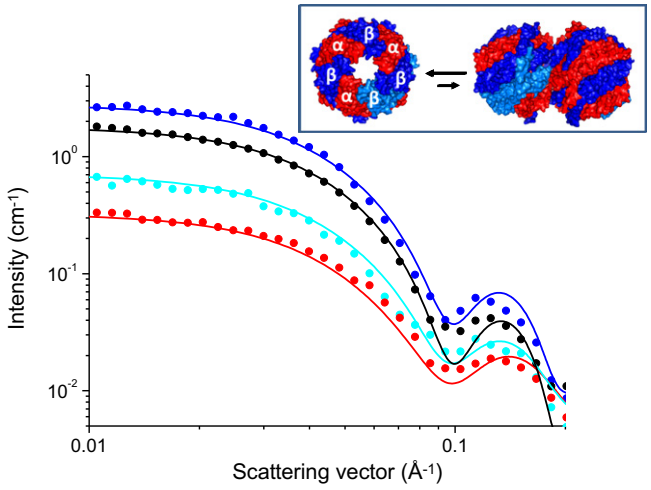

Fig. 1. Simulated (line) and experimental (dot) SANS profiles are shown for $PA28_{wt}$ composed of perdeuterated PA28α and non-deuterated PA28β in 0% (blue), 40% (cyan), and 98% (red) D_2O solutions along with those of non-deuterated $PA28_{wt}$ in 98% D_2O solution (black). The simulation was made based on the structural model shown in the inset: Three PAα and four PAβ subunits are alternatively arranged in the heteroheptameric ring in equilibrium between the single-ring (70%) and double-ring (30%) forms.

The observed gyration radius of the partially deuterated $PA28_{wt}$ oligomer was 41 Å in the D_2O solution, which was between those calculated from the models of SR^a (33 Å) and DR^a (49 Å). This indicated that the heteroheptameric rings were at equilibrium between the single- and double-ring forms, with populations of 70% and 30%, respectively. These data are consistent with our previous results obtained using $PA28_{\Delta\alpha loop}$ without deuteration [14], suggesting that the long insert region of PA28α has virtually no impact on the subunit assembly state of the PA28 hetero-oligomer [12]. SANS profiles calculated by taking into account the equilibrium between SR^a and DR^a were in excellent agreement with those experimentally obtained at four different contrasting points (Fig. 1).

3.3. Role of flexible loop of PA28α in proteasomal proteolysis

Our SANS data have provided a quantitative perspective of the $PA28_{wt}$ heterodimer except for the insert loops. To obtain structural information on these regions, we compared $^{1}H–^{15}N$ HSQC spectra between $PA28_{wt}$ and $PA28_{\Delta\alpha loop}$ in their uniformly ^{15}N-labeled forms. $PA28_{wt}$ exhibited limited numbers of HSQC peaks within a limited spectral region (Supplementary Fig. S5), implying that these peaks originated from considerably flexible segments of this large oligomer. The overlapping peaks mostly disappeared in the spectrum of $PA28_{\Delta\alpha loop}$, allowing us to assign them to the PA28α loops. Therefore, we observed that the PA28α loops were largely unstructured and highly mobile, which was consistent with the previous crystal structure of the PA28α homoheptamer that exhibited disordered insert segments [13].

To assess the functional role of the flexible loops of PA28α, we compared the time course of PA28-activated proteasomal degradation between $PA28_{wt}$ and $PA28_{\Delta\alpha loop}$ using 9–24-mer RLAkt peptides as model substrates. The results summarized in Fig. 2 clearly demonstrated that the 20S proteasome combined with $PA28_{wt}$ degraded longer peptides less efficiently although they possessed more cleavage sites. Interestingly, deletion of the PA28α loop facilitated the proteasomal degradation of longer peptides compared with $PA28_{wt}$-activated proteolysis. Consistent with

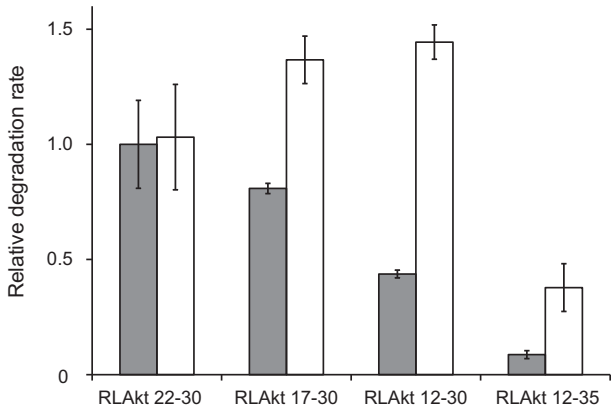

Fig. 2. Relative degradation rates are shown for various lengths of RLAkt peptides in the presence of the 20S proteasome activated by $PA28_{wt}$ (gray) or $PA28_{\Delta\alpha loop}$ (white). Values are means ± S.E. $n = 3$.

these observations, a 21-mer peptide derived from a melanoma differentiation antigen, ($TRP2_{355–375}$) was more efficiently degraded by the proteasome when the PA28α loops were absent (Supplementary Fig. S6). However, the proteasomal degradation of a small fluorogenic peptide, N-succinyl-LLVY-amido-4-methycoumarin, proceeded at almost identical rates when stimulated by $PA28_{wt}$ or $PA28_{\Delta\alpha loop}$ (Supplementary Fig. S7). The abovementioned effects of the PA28α loop deletion were most likely not appreciated in previous studies because small fluorogenic peptides were used as substrates, and the peptide degradation was analyzed after long incubation (12 h) [11,12].

In the alternative subunit arrangement of PA28, the flexible PA28α loops were assumed to have surrounded the central pore of its hexameric ring, serving as a gate for peptide entrance into the proteolytic chamber of the 20S proteasome. Our model suggests a functional role of these loops, which selectively act to hinder the passage of longer peptides while peptides as small as nonapeptides can pass through the passage.

The IFN-γ-inducible activator PA28 is involved in efficient production of antigenic peptides presented by MHC class I molecules [21,24]. PA28 enhances dual cleavage of peptide substrates giving rise to immunodominant epitopes without directly affecting the catalytic activities of the active sites inside the proteolytic chamber [24,25]. Interestingly, IFN-γ induces generation of a hybrid proteasome, in which the 20S proteasome is attached to both PA28 and PA700, as PA700–20S–PA28 [26]. This proteasome complex facilitates ATP-dependent degradation of larger protein substrates, which are assumed to enter the proteolytic chamber through the PA700-capped end. The resultant peptides may be further digested into shorter peptides in the other chamber capped by PA28. Based on our findings, an intriguing hypothesis is that the PA28α loops block the exit of the longer peptides from the proteolytic chamber to the extra-proteasomal medium until they are transformed to nonapeptides, which are suitable for antigen presentation by MHC class I molecule.

In summary, the present data have revealed that the PA28 heteroheptameric ring exhibits an alternative subunit arrangement in which the flexible PA28α loops act as gatekeepers in terms of size-selective transport of peptide substrates.

Acknowledgments

We would like to thank Dr. Richard K. Heenan for his kind help of SANS measurements at SANS2d of ISSI, which were performed under proposal No.RB720205. We also thank Ms. Kumiko Hattori for her help in preparation of recombinant proteins and Dr. Akira Sumiyoshi for his contribution at early stage of this study. This work was supported by Grants-in-Aid for Scientific Research on Innovative Areas (20107004 to K. Kato and 24113709 to M.S.) and Grant-in-Aid for Scientific Research (B) (24310068 to M.S.) and the Targeted Proteins Research Program from the Ministry of Education, Culture, Sports, Science, and Technology (to K. Kato and K.T.).

Appendix A. Supplementary data

Supplementary data associated with this article can be found, in the online version, at http://dx.doi.org/10.1016/j.bbrc.2013.01.071.

References

[1] J. Maupin-Furlow, Proteasomes and protein conjugation across domains of life, Nat. Rev. Microbiol. 10 (2012) 100–111.
[2] W. Baumeister, J. Walz, F. Zuhl, E. Seemuller, The proteasome: paradigm of a self-compartmentalizing protease, Cell 92 (1998) 367–380.
[3] B.M. Stadtmueller, C.P. Hill, Proteasome activators, Mol. Cell 41 (2011) 8–19.
[4] W. Dubiel, G. Pratt, K. Ferrell, M. Rechsteiner, Purification of an 11 S regulator of the multicatalytic protease, J. Biol. Chem. 267 (1992) 22369–22377.
[5] C.P. Ma, C.A. Slaughter, G.N. DeMartino, Identification, purification, and characterization of a protein activator (PA28) of the 20 S proteasome (macropain), J. Biol. Chem. 267 (1992) 10515–10523.
[6] B. Fabre, T. Lambour, J. Delobel, F. Amalric, B. Monsarrat, O. Burlet-Schiltz, M.P. Bousquet-Dubouch, Subcellular distribution and dynamics of active proteasome complexes unraveled by a workflow combining in vivo complex cross-linking and quantitative proteomics, Mol. Cell Proteomics (2012), http://dx.doi.org/10.1074/mcp.M112.023317.
[7] C. Realini, W. Dubiel, G. Pratt, K. Ferrell, M. Rechsteiner, Molecular cloning and expression of a γ-interferon-inducible activator of the multicatalytic protease, J. Biol. Chem. 269 (1994) 20727–20732.
[8] C. Realini, C.C. Jensen, Z. Zhang, S.C. Johnston, J.R. Knowlton, C.P. Hill, M. Rechsteiner, Characterization of recombinant REGα, REGβ and REGγ proteasome activators, J. Biol. Chem. 272 (1997) 25483–25492.
[9] M. Rechsteiner, C. Realini, V. Ustrell, The proteasome activator 11 S REG (PA28) and class I antigen presentation, Biochem. J. 345 (Pt 1) (2000) 1–15.
[10] E.J. Sijts, P.M. Kloetzel, The role of the proteasome in the generation of MHC class I ligands and immune responses, Cell Mol. Life Sci. 68 (2011) 1491–1502.
[11] X. Song, J. von Kampen, C.A. Slaughter, G.N. DeMartino, Relative functions of the α and β subunits of the proteasome activator, PA28, J. Biol. Chem. 272 (1997) 27994–28000.
[12] Z. Zhang, C. Realini, A. Clawson, S. Endicott, M. Rechsteiner, Proteasome activation by REG molecules lacking homolog-specific inserts, J. Biol. Chem. 273 (1998) 9501–9509.
[13] J.R. Knowlton, S.C. Johnston, F.G. Whitby, C. Realini, Z. Zhang, M. Rechsteiner, C.P. Hill, Structure of the proteasome activator REGα (PA28α), Nature 390 (1997) 639–643.
[14] M. Sugiyama, E. Kurimoto, Y. Morimoto, H. Sahashi, E. Sakata, K. Hamada, K. Itoh, K. Mori, T. Fukunaga, Y. Minami, K. Kato, Assembly state of proteasome activator 28 in an aqueous solution as studied by small-angle neutron scattering, J. Phys. Soc. Jpn. 78 (2009) 124802.
[15] R.K. Heenan, S.E. Rogers, D. Turner, A.E. Terry, J. Treadgold, S.M. King, Small angle neutron scattering using sans2d, Neutron News 22 (2011) 19–21.
[16] H.B. Stuhrmann, J. Haas, K. Ibel, M.H. Koch, R.R. Crichton, Low angle neutron scattering of ferritin studied by contrast variation, J. Mol. Biol. 100 (1976) 399–413.
[17] H.B. Stuhrmann, E.D. Duee, The determination of the scattering density distribution of polydisperse solutions by contrast variation: A neutron scattering study of ferritin, J. Appl. Cryst. 8 (1975) 538–542.
[18] M. Sugiyama, E. Kurimoto, H. Yagi, K. Mori, T. Fukunaga, M. Hirai, G. Zaccai, K. Kato, Kinetic asymmetry of subunit exchange of homooligomeric protein as revealed by deuteration-assisted small-angle neutron scattering, Biophys. J. 101 (2011) 2037–2042.
[19] A. Uenaka, T. Ono, T. Akisawa, H. Wada, T. Yasuda, E. Nakayama, Identification of a unique antigen peptide pRL1 on BALB/c RL male 1 leukemia recognized by cytotoxic T lymphocytes and its relation to the Akt oncogene, J. Exp. Med. 180 (1994) 1599–1607.
[20] M. Yagi-Utsumi, K. Matsuo, K. Yanagisawa, K. Gekko, K. Kato, Spectroscopic characterization of intermolecular interaction of Aβ molecules promoted on GM1 micelles, Int. J. Alzheimer's Dis. (2011). ID 950932.
[21] N. Shimbara, H. Nakajima, N. Tanahashi, K. Ogawa, S. Niwa, A. Uenaka, E. Nakayama, K. Tanaka, Double-cleavage production of the CTL epitope by proteasomes and PA28: role of the flanking region, Genes Cells 2 (1997) 785–800.
[22] Y. Sun, A.J. Sijts, M. Song, K. Janek, A.K. Nussbaum, S. Kral, M. Schirle, S. Stevanovic, A. Paschen, H. Schild, P.M. Kloetzel, D. Schadendorf, Expression of the proteasome activator PA28 rescues the presentation of a cytotoxic T lymphocyte epitope on melanoma cells, Cancer Res. 62 (2002) 2875–2882.

[23] Z. Zhang, A. Krutchinsky, S. Endicott, C. Realini, M. Rechsteiner, K.G. Standing, Proteasome activator 11S REG or PA28: recombinant REG α/REG β hetero-oligomers are heptamers, Biochemistry 38 (1999) 5651–5658.
[24] T.P. Dick, T. Ruppert, M. Groettrup, P.M. Kloetzel, L. Kuehn, U.H. Koszinowski, S. Stevanović, H. Schild, H.G. Rammensee, Coordinated dual cleavages induced by the proteasome regulator PA28 lead to dominant MHC ligands, Cell 86 (1996) 253–262.
[25] R. Stohwasser, U. Salzmann, J. Giesebrecht, P.M. Kloetzel, H.G. Holzhütter, Kinetic evidences for facilitation of peptide channelling by the proteasome activator PA28, Eur. J. Biochem. 267 (2000) 6221–6230.
[26] N. Tanahashi, Y. Murakami, Y. Minami, N. Shimbara, K.B. Hendil, K. Tanaka, Hybrid proteasomes. Induction by interferon-γ and contribution to ATP-dependent proteolysis, J. Biol. Chem. 275 (2000) 14336–14345.